X-nuclear MRS and MRI on a standard clinical proton-only MRI scanner

Yi-Fen Yen[a,*], Atsushi M. Takahashi[b], Jerome L. Ackerman[a]

[a]Athinoula A. Martinos Center for Biomedical Imaging, Department of Radiology, Massachusetts General Hospital, Harvard Medical School, Boston, MA, United States

[b]Department of Brain and Cognitive Sciences, McGovern Institute for Brain Research, Massachusetts Institute of Technology, Cambridge, MA, United States

Abstract

In light of the growing interest *in-vivo* deuterium metabolic imaging, hyperpolarized ^{13}C, ^{15}N, ^{3}He, and ^{129}Xe imaging, as well as ^{31}P spectroscopy and imaging in large animals on clinical MR scanners, we demonstrate the use of a (radio)frequency converter system to allow X-nuclear MR spectroscopy (MRS) and MR imaging (MRI) on standard clinical MRI scanners without multinuclear capability. This is not only an economical alternative to the multinuclear system (MNS) provided by the scanner vendors, but also overcomes the frequency bandwidth problem of some vendor-provided MNSs that prohibit users from applications with X-nuclei of low magnetogyric ratio, such as deuterium (6.536 MHz/Tesla) and ^{15}N (–4.316 MHz/Tesla). Here we illustrate the design of the frequency converter system and demonstrate its feasibility for ^{31}P (17.235 MHz/Tesla), ^{13}C (10.708 MHz/Tesla), and ^{15}N MRS and MRI on a clinical MRI scanner without vendor-provided multinuclear hardware.
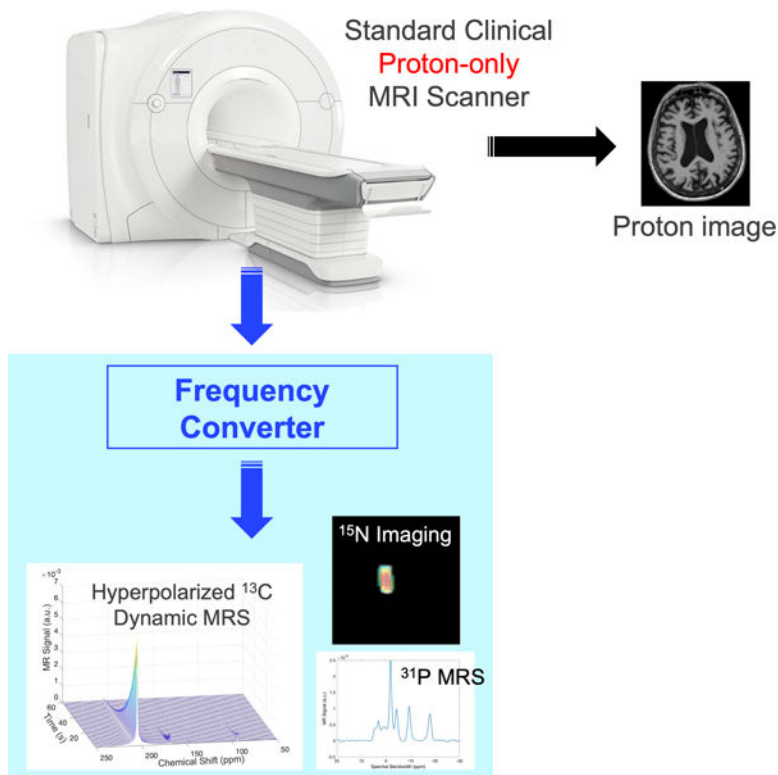
Graphical Abstract

*Corresponding author at: Athinoula A. Martinos Center for Biomedical Imaging, Massachusetts General Hospital, Bldg. 149, 13th Street, Room 2303A, Charlestown, MA, 02129, United States, yyen1@mgh.harvard.edu (Y.-F. Yen).

Keywords

Frequency converter; Magnetic resonance imaging; Magnetic resonance spectroscopy; Hyperpolarized MR; Multinuclear

Introduction

There is increasing interest in *in-vivo* deuterium metabolic imaging, ^{31}P spectroscopy of energy metabolism, hyperpolarized ^3He or ^{129}Xe gas imaging, and hyperpolarized ^{13}C or ^{15}N MR spectroscopy (MRS) and MR imaging (MRI) to assess metabolic flux into various metabolic pathways in animal and human research. While small bore high-field (preclinical) MR scanners typically have built-in capabilities for detecting signals from these non-proton nuclei (or X-nuclei), X-nuclear MR research involving large animals and humans is limited to special clinical MR scanners that are equipped with multi-nuclear systems (MNSs) provided by the scanner manufacturer. Yet, some of the major-vendor MNSs do not cover the frequencies of isotopes with low magnetogyric ratios, such as ^2H and ^{15}N. An alternative idea is to utilize a frequency converter to interface with the standard proton-only clinical scanner (with no MNS) to down-convert the proton RF frequency to the desired X-nuclear resonance frequency for RF excitation and up-convert the received X-nuclear signals to the proton carrier frequency to be recorded by the standard receiver chain of the clinical scanner.

Frequency conversion techniques were frequently used in early-day ultra-high field MRI systems. The original implementation of the 7T whole body MRI scanner at the

Massachusetts General Hospital utilized frequency conversion to interface a Siemens Sonata 64 MHz console to the 298 MHz RF front end of this instrument [1–5]. Similarly, frequency conversion enabled the interfacing of a Siemens Trio console (nominal operating frequency of 123 MHz) to a 619 MHz (14.56 T) Magnex animal magnet in this laboratory [6–9].

Frequency conversion techniques have also been used for proton high-resolution imaging and X-nuclear MRS/MRI on MR scanners of typical clinical field strengths. For example, proton microscopic imaging and hyperpolarized ^{3}He imaging were performed at 2T at Duke University using frequency conversion interface with a GE Signa 63 MHz console [10,11]. We have previously shown the utility of the frequency converter for ^{31}P solid-state MRI [12], and for scanning hyperpolarized ^{3}He gas on a 3T proton-only scanner [13].

The novelty of this frequency converter device is twofold: its inherent portability coupled with its minimal "invasiveness" in the sense that it requires essentially no scanner modifications and is relatively simple and quick to connect to a working scanner. These are key advantages especially in a busy clinical environment where workflow, performance and reliability are critical. Furthermore, clinical scanners must be maintained under service contracts, and not maintained by lab researchers and technicians as is often the case in many NMR and preclinical MRI labs. It is therefore important to minimize the risk of violating warranty and service contract terms as well as reducing the possibility of inadvertently leaving the scanner in an inoperative state after removing the device. The device is therefore designed to have minimal points of contact with the scanner hardware. The connections are primarily through the interface that is routinely used to connect RF coils.

To the best of the authors' knowledge, all prior art utilized the frequency conversion technique at system levels, not as a portable device. In this work, we will present a modern, portable design of the frequency converter system and demonstrate its utility in ^{31}P, ^{13}C and ^{15}N MRS and MRI on a clinical proton-only MR scanner.

Frequency converter design

A frequency converter system was assembled to interface with a Siemens Trio 3T MR clinical scanner (Siemens Healthineers, Erlangen, Germany) which was not equipped with multinuclear hardware. Fig. 1 illustrates schematic of the frequency converter setup for ^{15}N excitation and detection (Larmor frequency of 12.49 MHz at 3T). A low power replica of the ^{1}H transmit pulse at 123.23 MHz from table plug 1 (for local transmit/receive coils) is sampled with a Bird Electronic (Solon, OH) 553–75 75–150 MHz RF directional coupler element and 4230–059 line section terminating in a Bird 8201 500 watt 50 ohm dummy load capable of handling the full transmit power. The sampled low power ^{1}H pulse is "frequency mixed" with the appropriately chosen local oscillator (LO) frequency (110.74 MHz) from a Programmed Test Sources (Littleton, MA) PTS-160 frequency synthesizer in a Mini-Circuits (Brooklyn, NY) ZMY-2+ level 23 double balanced mixer. The frequency mixing process amounts to an analog multiplication of the two inputs to the mixer. For two sine wave inputs at frequencies ω_1 and ω_2, the output of the mixer is given by the trigonometric identity:

$$2\cos\omega_1 t\cos\omega_2 t = \cos(\omega_1 t + \omega_2 t) + \cos(\omega_1 t - \omega_2 t) \tag{1}$$

Thus, the two sine wave inputs to the mixer result in output sine waves at the sum and difference frequencies. Furthermore, any phase offset or amplitude variations of the input waves are preserved in the output waves. In any physically real mixer, a small amount of each input wave, harmonics of the inputs, as well as intermodulation products leak through to the output. A Mini-Circuits BBP-10.7+ bandpass filter on the output of the mixer selects the correct 12.49 MHz spectrally pure sideband while rejecting undesired leakage frequencies. This filtered output signal is an exact replica of the proton transmit pulse except now at the ^{15}N frequency; it carries all of the phase and amplitude variations of the original ^{1}H pulse.

Although the filter's center frequency is not precisely at the 12.49 MHz Larmor frequency of ^{15}N, it works extremely well and is an order of magnitude less expensive than purchasing a custom-made filter at the exact frequency. Any excess insertion loss at the ^{15}N frequency is readily made up by the gain of the RF power amplifier (RFPA). Note that the sum frequency sideband (233.97 MHz) as well as the carrier frequencies and their harmonics are far out of the filter passband and are therefore fully rejected, leaving a spectrally pure RF pulse. More discussion of the choice of bandpass filters is found in the Supplementary Material accompanying this article. The ^{15}N RF pulse is then routed to an alternative RFPA, an Electronic Navigation Industries (ENI, Rochester, NY) LPI-10 1 kW linear amplifier, rather than the scanner's RFPA, and then to a custom T/R switch and RF coil.

To guard against any spurious frequency content in the scanner's original ^{1}H RF pulse inadvertently mixing into the filter passband and interfering with ^{15}N excitation or reception, the ^{1}H RF pulse replica is passband filtered at 123 MHz before being applied to the mixer.

An analogous arrangement is used on the receive side of the frequency converter: the ^{15}N signal from the low noise preamp is mixed to the proton frequency in a second double balanced mixer, filtered to select the sideband at the proton frequency, and routed to the scanner receiver. The frequency converter is located next to the scanner electronic cabinets while the ^{15}N preamplifier is located near the RF coil in the magnet. To power the preamplifier, DC of 12 volts is multiplexed onto the same coaxial cable used to route the ^{15}N RF signal from the preamplifier to the frequency converter with a bias tee. Following the bias tee are two gain stages (Mini-Circuits ZFL-500-BNC, about 24 dB gain each), followed by bandpass filtering (Mini-Circuits BBP-10.7+) and mixing back to the ^{1}H frequency. The output of the mixer is bandpass filtered (model 6BL10-127.27/T5-B/B, K&L Microwave, Salisbury, MD) and routed to the scanner receiver through table plug 1.

To preserve as much dynamic range as possible in both the excitation pulse and the received signal, "level 23″" mixers are used, meaning they are driven by a local oscillator signal at about 23 dBm (about 0.2 W) or higher. This permits rather high levels of MR signal on the other input to the mixer to be converted without distortion. To enable this high-level mixer drive, the PTS LO output of around 3 dBm is boosted with a Mini-Circuits ZHL-3A amplifier (maximum output 29.5 dBm) and split to each mixer with a Mini-Circuits ZSC-2-1W+ power divider. Attenuators are used in various locations in the circuit chain to achieve the proper signal levels at each stage.

The low noise preamplifier uses a Mini-Circuits PHA-13LN+ GaAs-FET low noise RF amplifier chip biased at 5VDC and embedded in a passive T/R switch employing crossed diodes and a pi-circuit lumped element quarter wave line; a coaxial line at this very low frequency would be electrically lossy and physically unwieldy. For ^{13}C, the same set up was used except different bandpass filters (Mini-Circuits BBP-30+), a different LO frequency from the PTS-160 to yield a 31.00 MHz sideband, and a different low-noise preamplifier (Advanced Receiver Research, Burlington CT) were used.

The un-blank logic signal to the ENI RFPA is derived by splitting off the fiber optic un-blank signal of the Siemens console and converting it to Transistor-Transistor Logic (TTL). The signal that un-blanks the scanner's standard RFPA and puts it in transmit mode is supplied on a fiber optic connection from the sequencer hardware. The un-blank signal is also required by the frequency shifted RFPA. We used standard fiber to TTL converters (Broadcom part numbers: AFBR-1624Z and AFBR2624Z) to convert the optical signal to a TTL signal used by the frequency converter RFPA. This TTL signal is also used to recreate an optical signal which is fed back to the scanner's RFPA. The propagation delay is 30 nanoseconds and is sufficiently short to ensure both RFPA are un-blanked prior to the RF excitation pulse.

The T/R switch illustrated in Fig. 1 is a classic passive design relying on the transmit RF pulse power to switch simple (*e.g.*, 1N914B) silicon diodes between conductive and nonconductive states. This switch was easy to implement, worked extremely fast (in nanoseconds), and was essential for ZTE of short T2 tissues such as solid bone [12]. Actively driven T/R switches based on PIN diodes exhibit superior on/off ratios and are standard in clinical MRI scanners. All the data in this report (Fig. 2–5) were acquired with an actively driven T/R switch using non-magnetic PIN diodes (MA4P7435NM by MACOM Technology Solutions, Massachusetts, USA).

Experimental

The feasibility of the frequency converter system was demonstrated with MRS/MRI of a thermal ^{15}N phantom (*i.e.* non-hyperpolarized) and a ^{13}C thermal phantom, dynamic spectroscopy of a hyperpolarized [2–^{13}C]pyruvate phantom, and *in vivo* ^{31}P MRS of a rat head. A pulse- and-acquire FID sequence with a hard excitation pulse was used to acquire MRS and dynamic spectroscopy data. A gradient echo (GRE) sequence was used with altered fields of view and slice thicknesses to account for the difference between the magnetogyric ratios of the X-nucleus and proton. In all cases, standard proton pulse sequences were used; the scanner does not "know" it was in fact exciting and acquiring multinuclear signals. For this reason, pulse sequence parameters relating to the magnetogyric ratio (such as scanner frequency, field of view, slice thickness, and chemical shift scales) are incorrectly excited or labeled because the scanner software does not take the substitution of magnetogyric ratio into account. The user must make the adjustment by specifying altered values for these parameters to achieve the desired values.

Thermal ^{15}N and ^{13}C phantom experiments

The ^{15}N thermal phantom was made of 2.4 mL 3 M ^{15}N-labeled imidazole in a plastic tube of 1.1 cm in diameter and 2.5 cm in length. The ^{13}C thermal phantom was made of 1.8 mL 9.3 M [1–^{13}C]pyruvate with 10 mM trityl (OX63, Oxford Instruments, UK) in an Eppendorf tube. Both phantoms were doped with a small amount of gadolinium (Magnevist, Bayer Healthcare, Germany) to shorten T_1 relaxation times. Two custom-made solenoid coils (1 cm in inner-diameter and 4 cm in length), one tuned to the ^{15}N frequency and the other to the ^{13}C frequency, were used for the ^{15}N and ^{13}C experiments, respectively. A standard GRE sequence provided by the scanner vendor for proton imaging was used to prescribe a scan of the ^{15}N phantom with the following scanning parameters: TR/TE/FA = 2000 ms/5.69 ms/90°, field of view (FOV) = 32 mm × 32 mm (corresponding to an actual FOV of 324 mm × 324 mm for ^{15}N), matrix size = 64 × 64, spatial resolution = 5.1 mm × 5.1 mm for ^{15}N, a single 2.5 mm axial slice (corresponding to a $2.5 × 42.5775/4.316 = 24.7$ mm slice for ^{15}N) covering the whole ^{15}N phantom, receiver bandwidth = 90 Hz/pixel, 4 averages, and a total scan time of 8 min and 32 s. GRE data of the ^{13}C phantom was collected using the following scanning parameters: TR/TE/FA = 100 ms/5.14 ms/90°, FOV = 50.3 mm × 50.3 mm (corresponding to an actual FOV of 200 mm × 200 mm for ^{13}C), matrix size = 64 × 64, spatial resolution = 3.1 mm × 3.1 mm for ^{13}C, a single 4 mm coronal slice (corresponding to a $4 × 42.5775/10.708 = 15.9$ mm slice for ^{13}C), receiver bandwidth = 260 Hz/pixel, 32 averages, and a total scan time of 3 min and 25 s. Flip angle calibration was performed on the scanner using the standard manual pre-scan procedure. For the purpose of image display, T_1-weighted proton images were acquired on these phantoms by carefully replicating the phantom positions inside a custom-made proton saddle coil.

Hyperpolarized ^{13}C phantom experiment

A [2–^{13}C]pyruvate sample consisting of 18 μL of >99.0% ^{13}C-enriched neat [2–^{13}C]pyruvic acid (MilliporeSigma, Massachusetts, USA) and 30 mM trityl AH111501 (Polarize, ApS, Denmark) was hyperpolarized in a 6.7 T D-DNP [14] polarizer (SpinAligner, Polarize, Denmark) for one hour. A 3 mL syringe filled with 2 mL 70% isopropyl alcohol (MilliporeSigma, Massachusetts, USA) was used for localization and frequency calibration. The custom-made ^{13}C solenoid coil described above was used for this experiment. After one hour of polarization buildup, hyperpolarized [2–^{13}C]pyruvate sample was dissolved rapidly in 3.2 mL dissolution medium, which was prepared in a 1 liter stock consisting of 100 mg of disodium EDTA dihydrate, 5.96 g of Trizma PreSet Crystals pH 7.6 (Sigma-Aldrich T7943), 2.92 g of sodium chloride (NaCl), and 3.20 g of sodium hydroxide (NaOH) to 1 L of distilled H_2O. After dissolution, 2 mL of dissolved hyperpolarized [2–^{13}C]pyruvate solution was collected in a 3 mL syringe, de-gassed, rapidly delivered to the 3T clinical scanner, and placed vertically inside the ^{13}C solenoid coil at the isocenter. Time from dissolution to the start of acquisition was approximately 30 s. The degree of polarization at the start of acquisition was approximately 40%. Dynamic spectroscopy was acquired with a pulse-and-acquire FID sequence repeated every 3 s (TR) for 3 min with a 10° flip angle, 20,000 Hz spectral bandwidth, and 4096 spectral points. Data reconstruction was performed offline by using custom-made scripts in MATLAB (The MathWorks Inc., Massachusetts, USA). The complex raw data were line-broadened by 10 Hz with no zero fill.

In vivo ^{31}P experiment

^{31}P MRS was performed in an anesthetized Sprague-Dawley rat (Charles River Laboratories International, Inc., Massachusetts, USA) by using an inductively coupled single-loop ^{31}P coil of 2 cm in diameter placed on the top of the rat head [15]. Power calibration of the ^{31}P coil was performed, prior to the animal experiment, on a 50 mL 2 M monophosphate phantom dopped with 500 uL of gadolinium to shorten the ^{31}P T_1 relaxation time. The animal was positioned in an MRI-compatible stereotaxic cradle, with a nose cone connected to an isoflurane vaporizer (2% isoflurane in 30% enriched air). The animal's respiration rate was maintained at approximately 35–40 breaths per minute and monitored visually throughout the experiment. A ^{31}P spectrum was acquired from the rat head with the pulse-and-acquire FID sequence with TR of 3 s, 90° flip angle, 8000 Hz spectral bandwidth, 4096 spectral points, and 400 averages for a durationof 20 min. Data reconstruction was performed offline by using custom-made scripts in MATLAB. The complex raw data were line-broadened by 50 Hz, no zero fill, phased with 0th and 1st order phases, and baseline corrected. After the experiment, the animal was fully recovered before being transferred back to the animal facility. The animal experiment was performed in accordance with a protocol approved by the Institutional Animal Care and Use Committee of Massachusetts General Hospital.

Results

The ^{15}N image and spectrum of the ^{15}N-imidazole phantom acquired by using the frequency converter are shown in Fig. 2, in which the ^{15}N image (in color) is superimposed on the T_1-weighted proton image (in gray scale). The imidazole molecule is a planar 5-membered ring containing two nitrogen atoms; both were labeled with ^{15}N. Because hydrogen can bind to either nitrogen, the two occur in equivalent tautomeric forms, and thus appear as a single peak in the ^{15}N MR spectrum. The ^{13}C image and spectrum of the [1–^{13}C]pyruvate phantom are shown in Fig. 3. Both the [1–^{13}C]pyruvate and its hydrate form appear in the ^{13}C spectrum.

The spectrum of hyperpolarized [2–^{13}C]pyruvate solution shows the [2–^{13}C]pyruvate peak (206 ppm), [1–^{13}C]pyruvate doublet (171 ppm), and [2–^{13}C]pyruvate-hydrate (93 ppm), as expected [16] (Fig. 4**A**). The [1–^{13}C]pyruvate doublet is due to J_{CC} coupling between the 1.1% natural abundant ^{13}C at the C1 position and the enriched, hyperpolarized ^{13}C at the C2 position. ^{13}C-pyruvate-hydrate usually appears in the spectrum of ^{13}C-pyruvate solution, such as in Fig. 2. In the hyperpolarized [2–^{13}C]pyruvate experiment, the [1–^{13}C]pyruvate-hydrate is simply too small to be detected. Small impurities (148 ppm and 240 ppm) are also observed in the ^{13}C spectrum. The stack plot (Fig. 4**B**) shows exponential delays due to T_1 relaxations and RF depletions. T_1 relaxation times are approximately 50 s, 68 s, and 66 s for [2–^{13}C]pyruvate, [1–^{13}C]pyruvate, and [2–^{13}C]pyruvate-hydrate, respectively, after corrections for the flip angles.

The *in vivo* ^{31}P spectrum of a rat head shows multiple ^{31}P peaks (as labeled in Fig. 5) typically observed from brain and muscle (in the head surrounding the brain) [17]. Phosphocreatine (PCr) and the three adenosine triphosphate (ATP) peaks are well separated. The phosphodiesters (PDE), inorganic phosphate (P_i), and phosphomonoesters (PME) peaks

are somewhat overlapping but likely quantifiable by curve fitting. The quality of the ^{31}P spectrum from a 20-min acquisition of a live rat on the standard clinical MR scanner is highly encouraging.

Discussion

We have demonstrated MRS and MRI of ^{13}C and ^{15}N thermal phantoms, hyperpolarized ^{13}C dynamic spectroscopy, and *in vivo* ^{31}P MRS on a clinical proton-only 3T scanner by using a custom-made frequency converter system. This offers possibilities for multiple attractive applications, including deuterium metabolic imaging, hyperpolarized ^{13}C or ^{15}N MR spectroscopic imaging, and ^{31}P MRS to study metabolism in small and large animals, on standard clinical 3T scanners.

Other than adding multinuclear imaging and spectroscopy capability to proton-only scanners, there are additional advantages offered by the frequency converter. In the case of reference [12], which involved ^{31}P ZTE imaging of very short T_2 solid-state signals from bone mineral, the multinuclear accessory on that scanner had a minimum receiver recovery time (the time from the end of an RF pulse to when the MR signal is valid) that was far too long to capture the rapidly decaying MR signal. In contrast, the proton channel of the scanner exhibited a receiver recovery time on the order of 5 μs, more than adequate to carry out solid-state ZTE acqusitions. The frequency converter permitted these acqusitions via the proton channel. In the case of references [6–9] a frequency converter enabled a 3T Siemens console to be used with a 15T magnet.

There is a vast library of imaging and spectroscopy pulse sequences developed for proton MR, whereas the array of sequences for other isotopes is very limited, and typically requires special coding and substantial effort. The frequency converter permits researchers to utilize the existing library of sequences developed for protons, with the limitation that adjustments in distance and frequency related parameters must be made to account for the difference in magnetogyric ratios.

The interface between the frequency converter and the scanner is made at the patient table connector for local T/R coils; the only additional scanner signal access required is to the RF un-blank logic signal. The frequency converter fits in a portable cart. Because of the simplicity of connecting the frequency converter to the scanner and the limited number of "points of contact," the frequency converter may be readily shared among multiple scanners at multiple field strengths. Changing the frequency of operation requires changing a pair of bandpass filters for either the x-nucleus channel of the frequency converter (and also for the proton channel if the B_0 field is changed).

Although the present implementation of the frequency converter utilizes discrete coaxial RF devices, significant miniaturization is possible with printed circuit board devices or with digital mixing. Either analog or digital single sideband mixing may reduce or obviate the need for analog bandpass filters. In principle, the use of single sideband or digital mixing would provide performance improvements such as reduced spurious frequency interference and increased dynamic range. However, in practice, the signal-to-noise ratio, and therefore

the dynamic range, of heteronuclear MR signals is typically low, limiting some of the potential advantage of these implementations. Miniaturization would be an advantage when expanding the frequency converter to multiple receive channels.

The frequency converter offers a viable low cost option for adding multinuclear capability to a proton-only scanner, and for sharing the device among multiple scanners with a range of field strengths. Although purchasing a multinuclear accessory from the scanner vendor would be the first choice for adding multinuclear capability to a scanner, this is generally quite expensive in comparison with the frequency converter. In addition, the vendor built-in multinuclear hardware on a dedicated clinical scanner is only utilized for a small fraction of time (as compared to proton imaging). In comparison, the frequency converter is portable and can be transferred to any clinical scanner when multinuclear MRS/MRI is needed on that system. Furthermore, the scanner vendor's multinuclear accessory may be limited to a small number of predetermined isotopes, not necessarily the particular isotope of interest to the experimenter and may come with a limited number of pulse sequences that work with it. In principle, the frequency converter permits any proton pulse sequence to be used on any isotope, given the limitations relevant to dimensional scaling discussed above.

The frequency converter must be reconfigured by exchanging the X-nucleus bandpass filters when changing isotopes. A typical workflow could start with proton MRI using the normally configured scanner, and then be followed by connecting the frequency converter to acquire a ^{31}P spectrum. Once the frequency converter is connected, it can be reconfigured by swapping filters and the RF coil (and preamps and T/R switches if they are narrowband) to measure yet a third isotope. The time ordering of the isotopes and whether the measurement is of an image or spectrum are immaterial.

We have not addressed the safety issue of specific absorption rate (SAR) that is relevant for human studies. A pair of frequency converter stages for the forward and reverse RF power at the transmit coil sampled at the X-isotope frequency via directional couplers can be added to convert these waveforms to the proton frequency, and then supplied to the scanner hardware for real-time SAR monitoring or supplied to a separate SAR monitoring device. However, this does not substitute for the SAR modeling performed by the scanner software before the scan starts. SAR is considerably reduced for X-isotopes and therefore of less concern because of their lower frequency.

Nor was a decoupling channel provided for the frequency converter. Proton decoupling is often part of spectroscopic sequences, particularly for ^{13}C, to simplify spectra and promote nuclear Overhauser enhancement. A separate proton CW decoupling channel can readily be added to the frequency converter, but programming more complex pulse sequences such as gated or composite pulse decoupling involves additional challenges.

Conclusion

A portable frequency converter was designed to permit X-nucleus MR imaging and spectroscopy on a clinical proton-only MRI scanner. It was successfully tested with images and spectra of ^{13}C and ^{15}N enriched thermal phantoms, a hyperpolarized ^{13}C phantom, and

in vivo ^{31}P MRS. The SNR of the receiver system is determined mostly by the coil, T/R switch and preamplifier. Signal levels in the frequency converter are chosen to be well above their noise floor and will only minimally increase overall noise. With the construction of the hardware demonstrated here as a prototype, we are positioned to miniaturize the frequency converter further, expand the design to multi-channels, develop compatibility with all major vendor clinical platforms, and explore large animal as well as human applications in the future.

Supplementary Material

Refer to Web version on PubMed Central for supplementary material.

Acknowledgements

Data availability

Data will be made available on request.

Abbreviations:

MRI	magnetic resonance imaging
MRS	magnetic resonance spectroscopy
MNS	multinuclear system
RFPA	RF power amplifier
TTL	transistor-transistor logic
GRE	gradient echo
T/R	transmit/receive
PCr	phosphocreatine
PME	phosphomonoesters
PDE	phosphodiesters
ATP	adenosine triphosphate
P$_i$	inorganic phosphate

References

[1]. Augustinack JC, van der Kouwe AJW, Blackwell ML, Salat DH, Wiggins CJ, Frosch MP, et al. , Detection of entorhinal layer II using Tesla magnetic resonance imaging, Ann. Neurol 57 (4) (2005) 489–494, 10.1002/ana.20426. [PubMed: 15786476]

[2]. Kelley DAC, Hardware Considerations in Ultra High Field MRI. Ultra High Field Magnetic Resonance Imaging, Springer US, Boston, MA, 2006, pp. 45–57.

[3]. Polimeni JR, Hinds OP, Balasubramanian M, van der Kouwe AJW, Wald LL, Dale AM, et al. , Two-dimensional mathematical structure of the human visuotopic map complex in V1, V2, and V3 measured via fMRI at 3 and 7 Tesla, J. Vis 5 (8) (2005) 898, 10.1167/5.8.898. –.

[4]. Wald LL, Wiggins GC, Potthast A, Wiggins CJ, Triantafyllou C, Design considerations and coil comparisons for 7 T brain imaging, Appl. Magn. Reson 29 (1) (2005) 19, 10.1007/BF03166954.

[5]. Wiggins GC, Potthast A, Triantafyllou C, Wiggins CJ, Wald LL, Eight-channel phased array coil and detunable TEM volume coil for 7 T brain imaging, Magn. Reson. Med 54 (1) (2005) 235–240, 10.1002/mrm.20547. [PubMed: 15968650]

[6]. Burns JA, Botelho JL, Bell JI, Faquin W, Lopez-Guerra G, Ackerman JL, et al. , Injectable aorta tissue paste for vocal fold medialization: residence time, biocompatibility, and comparison to predicates in a guinea pig subdermal model, Ann. Otol. Rhinol. Laryngol 125 (11) (2016) 900–911, 10.1177/0003489416660114. [PubMed: 27440067]

[7]. Cohen O, Ackerman JL, Ex vivo mouse brain microscopy at 15T with loop-gap RF coil, Magn. Reson. Imaging 51 (2018) 1–6, 10.1016/j.mri.2018.04.010. [PubMed: 29679634]

[8]. Cortes ARG, Cohen O, Zhao M, Aoki EM, Ribeiro RA, Abu Nada L, et al. , Assessment of alveolar bone marrow fat content using 15 T MRI, Oral. Surg. Oral. Med. Oral. Pathol. Oral. Radiol 125 (3) (2018) 244–249, 10.1016/j.oooo.2017.11.016. [PubMed: 29292160]

[9]. Lim C-LSP, Ackerman JL, Pre-amplifiers for a 15-Tesla magnetic resonance imager, in: IEEE International RF and Microwave Conference (RFM), Penang, Malaysia, 2013, pp. 295–299.

[10]. Johnson GA, Cofer GP, Hedlund LW, Maronpot RR, Suddarth SA, Registered (1)H and (3)He magnetic resonance microscopy of the lung, Magn. Reson. Med 45 (3) (2001) 365–370, 10.1002/1522-2594(200103)45:3<365::aid—mrm1047>3.0.co;2-0. [PubMed: 11241691]

[11]. Shattuck MD, Gewalt SL, Glover GH, Hedlund LW, Johnson GA, MR microimaging of the lung using volume projection encoding, Magn. Reson. Med 38 (6) (1997) 938–942, 10.1002/mrm.1910380613. [PubMed: 9402195]

[12]. Wu Y, Reese TG, Cao H, Hrovat MI, Toddes SP, Lemdiasov RA, et al. , Bone mineral imaged *in vivo* by 31P solid state MRI of human wrists, J. Magn. Reson. Imaging 34 (3) (2011) 623–633, 10.1002/jmri.22637. [PubMed: 21761459]

[13]. Hinton DPVJ, Ackerman JL, Massey JE, Carberry JA, Pomeroy VR, Hersman FW, Tseng CH, Walsworth RL, in: Hyperpolarized 3He imaging on a 3 Tesla whole body MRI Fortieth Experimental NMR Conference, Orlando, FL, 1999.

[14]. Ardenkjaer-Larsen JH, Bowen S, Petersen JR, Rybalko O, Vinding MS, Ullisch M, et al. , Cryogen-free dissolution dynamic nuclear polarization polarizer operating at 3.35 T, 6.70 T, and 10.1 T, Magn. Reson. Med 81 (3) (2019) 2184–2194, 10.1002/mrm.27537. [PubMed: 30357898]

[15]. Takahashi Atsushi M., D. G, Hardy Erin E., Miller Julie, Wakimoto Hiroaki, Cahill Daniel P., Yen Yi-Fen, Inductively coupled floating coil for hyperpolarized 13C imaging of mouse brain, , editor, in: The 31th Annual Meeting of the International Society of Magnetic Resonance in Medicine; Virtual, ISMRM, 2022, p. 3531.

[16]. Malloy CR, Maher E, Marin-Valencia I, Mickey B, DeBerardinis RJ, Dean Sherry A, Carbon-13 nuclear magnetic resonance for analysis of metabolic pathways, in: Sweedler JV, Lutz NW, Wevers RA (Eds.), Methodologies For Metabolomics: Experimental Strategies and Techniques, Cambridge University Press, Cambridge, 2013, pp. 415–445.

[17]. Liu Y, Gu Y, Yu X, Assessing tissue metabolism by phosphorous-31 magnetic resonance spectroscopy and imaging: a methodology review, Quant. Imaging Med. Surg 7 (6) (2017) 707–726, 10.21037/qims.2017.11.03. [PubMed: 29312876]
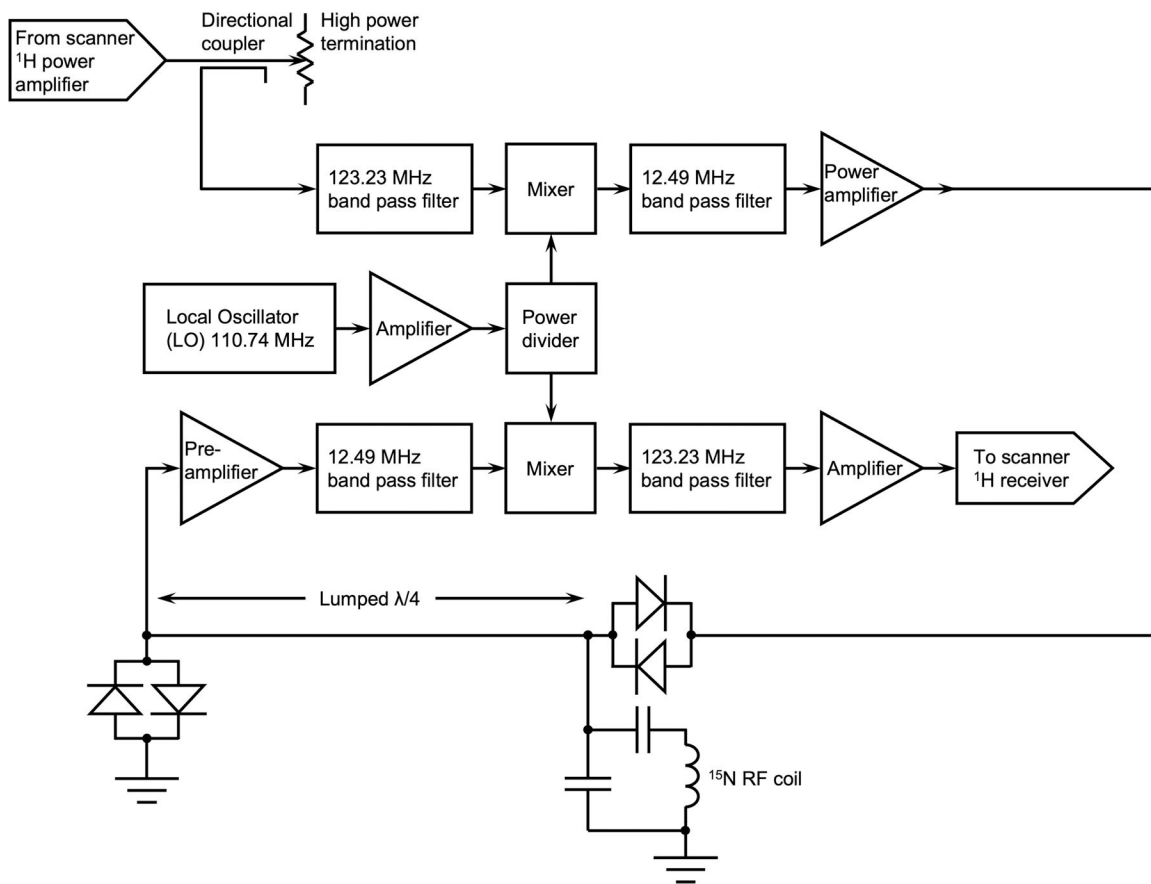
Fig. 1.
Simplified schematic diagram of the frequency converter circuit for ^{15}N MR. The ^{1}H transmit pulse from the scanner is mixed with a local oscillator (LO) frequency from a synthesizer to translate the pulse to the ^{15}N frequency, which is amplified by an RF power amplifier and sent to the coil for ^{15}N excitation. The ^{15}N MR signal detected by the coil is amplified by a low noise preamplifier, mixed with the LO to translate it to the ^{1}H frequency, and routed to the scanner ^{1}H receiver. For simplicity, other amplifiers, attenuators, filters, bias tees, etc., are not shown.
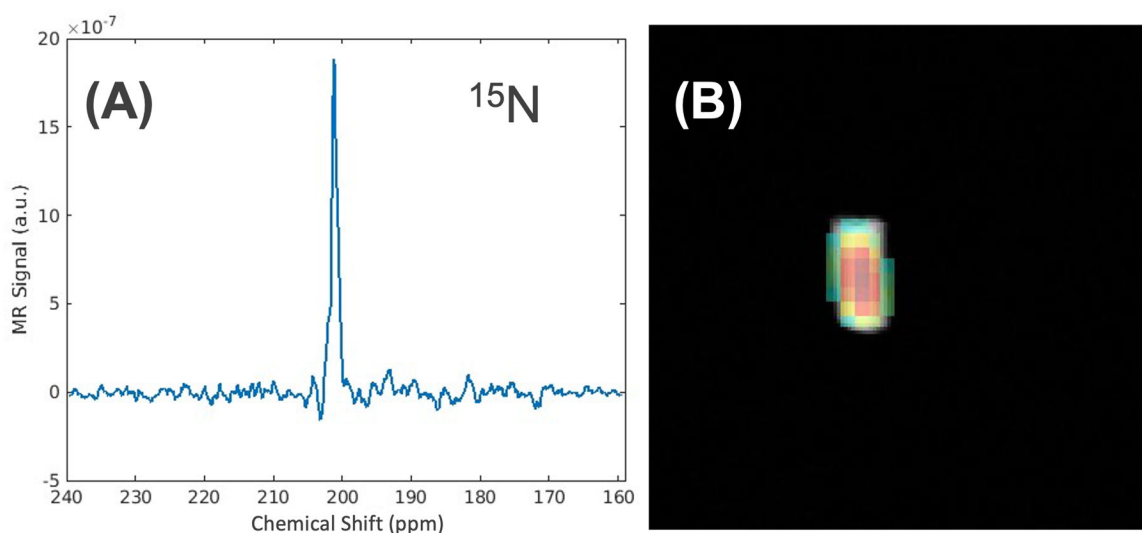
Fig. 2.
[15]N spectrum and image of ^{15}N-imidazole using the frequency converter interfaced to a clinical 3T MR scanner that was not equipped with multinuclear hardware. (A) ^{15}N MR spectrum of doubly labeled ^{15}N-imidazole, which is a planar 5-membered ring containing two nitrogens. Because hydrogen can bind in rapid exchange to either ^{15}N atom, the two ^{15}N atoms are in equivalent tautomeric forms and thus, appear as a single peak in the ^{15}N MR spectrum. (B) Axial ^{15}N image (color) of the ^{15}N-imidazole phantom superimposed on its T_1-weighted proton image (gray scale).
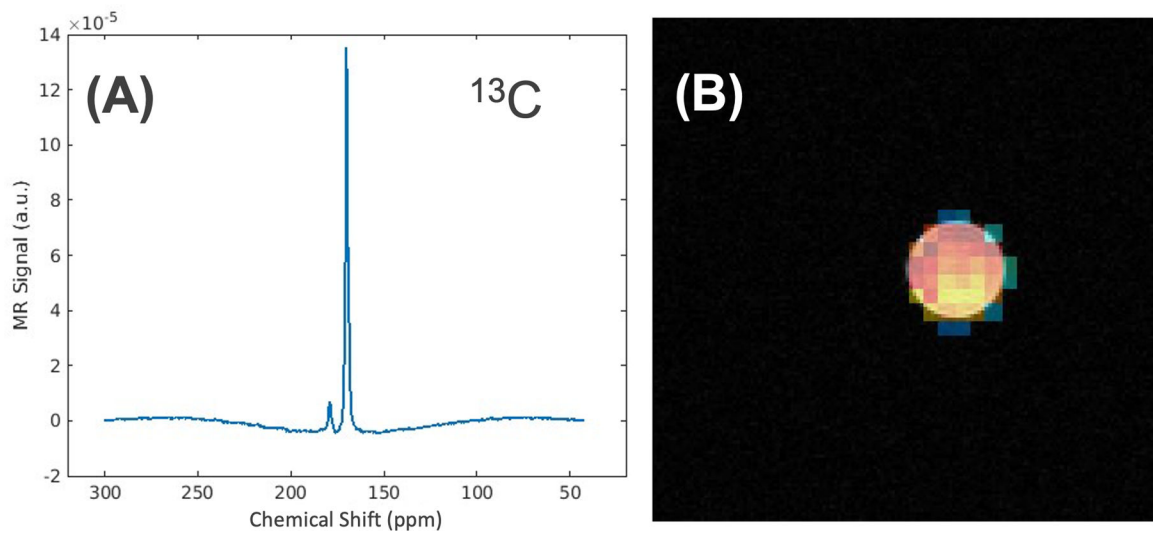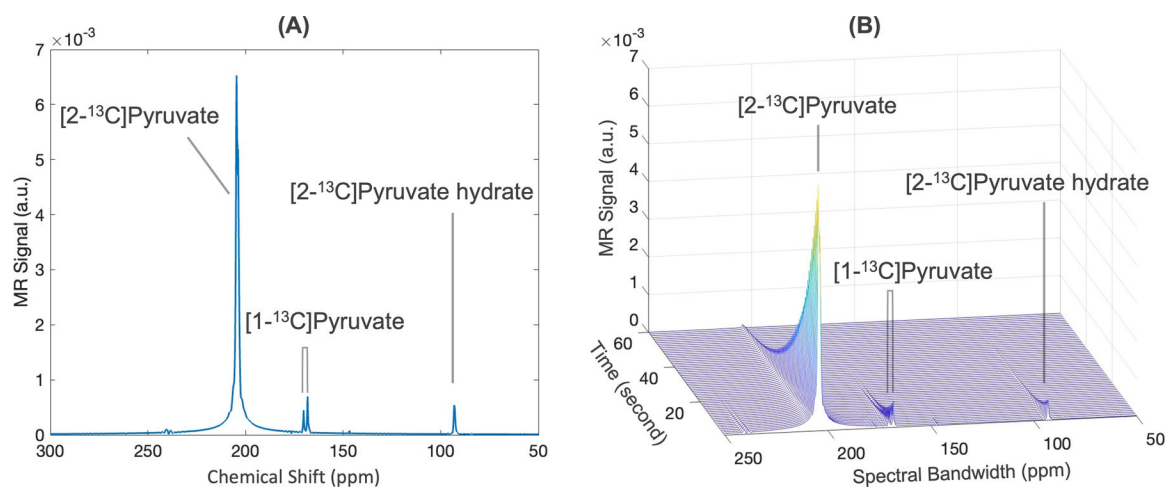
Fig. 3.
^{13}C spectrum and image of [1–^{13}C]pyruvate using the frequency converter interfaced to a clinical 3T MR scanner that was not equipped with multinuclear hardware. (A) ^{13}C MR spectrum showing [1–^{13}C]pyruvate and its hydrate form (small peak). (B) Coronal ^{13}C image (color) of the [1–^{13}C]pyruvate phantom superimposed on its T_1-weighted proton image (gray scale).

Fig. 4.
^{13}C spectrum (A) and signal decay (B) of hyperpolarized [2–^{13}C]pyruvate solution acquired using the frequency converter interfaced to a standard protononly clinical 3T MR scanner. (A) ^{13}C MR magnitude spectrum of the first time frame showing [2–^{13}C]pyruvate, its hydrate form, and a [1–^{13}C]pyruvate doublet from the natural abundant ^{13}C J_{CC} coupled to the hyperpolarized enriched [2–^{13}C]pyruvate. (B) Stack plot of dynamic spectroscopy showing the hyperpolarized signal decay via T_1 relaxation.
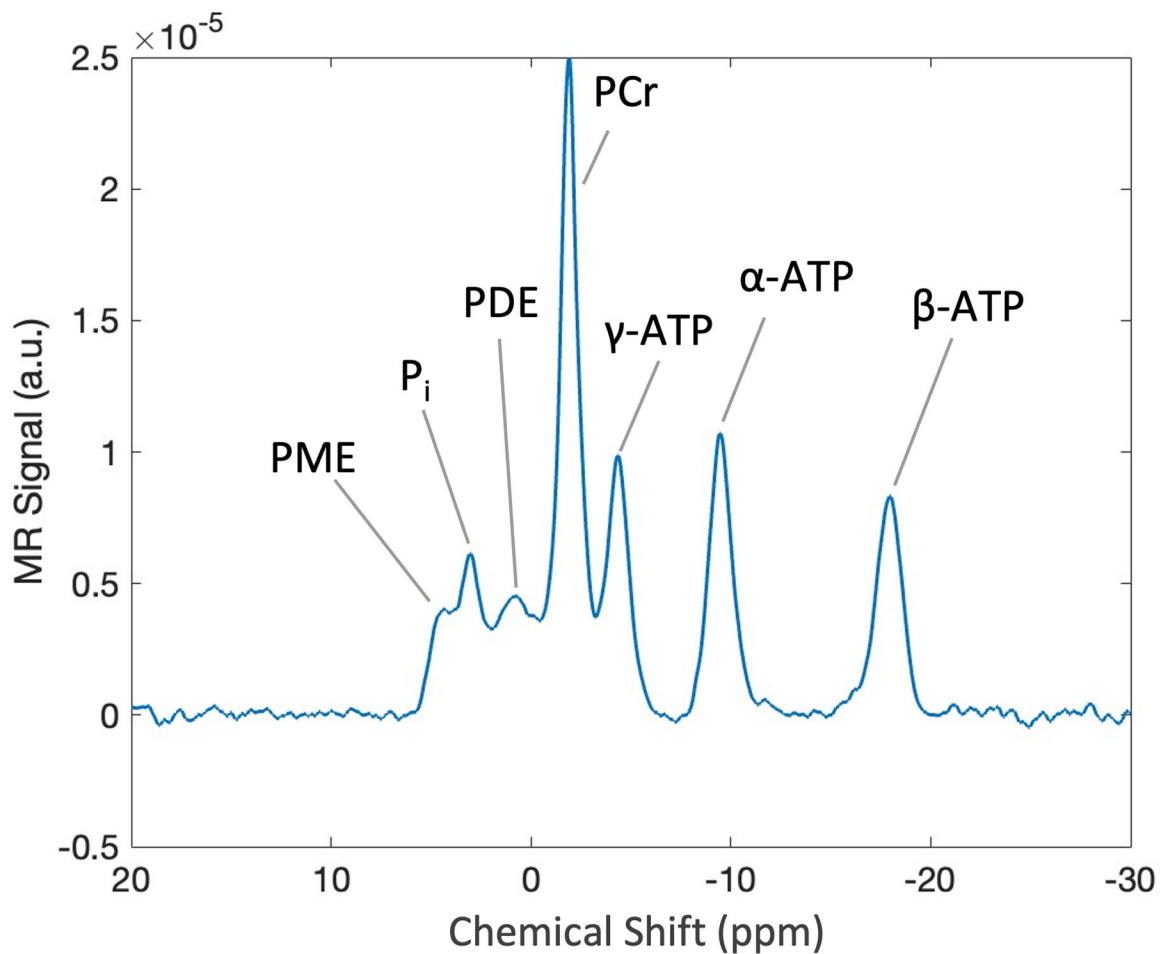
Fig. 5.
In vivo ^{31}P spectrum of a rat head acquired in 20 min by using the frequency converter interfaced to a standard proton-only clinical 3T MR scanner. The spectrum was phased and background corrected. [31]P peaks typically observed in the head are shown here including phosphocreatine (PCr), three adenosine triphosphate (ATP) peaks, phosphodiesters (PDE), inorganic phosphate (P_i), and phosphomonoesters (PME).